BNL-67884-01/07-Rev.

RETRIEVAL OF AEROSOL PROPERTIES FROM MOMENTS OF THE PARTICLE SIZE DISTRIBUTION FOR KERNELS INVOLVING THE STEP FUNCTION: CLOUD DROPLET ACTIVATION

D. L. Wright[1], Shaocai Yu[1], P. S. Kasibhatla[1], R. McGraw[2], S. E. Schwartz[2], V. K. Saxena[3], and G. K. Yue[4]

Revised: July 2001

Published in
Journal of Aerosol Science 33, 319–337 (2002)

[1] Nicholas School of the Environment, Duke University, Durham, NC 27708.
[2] Atmospheric Sciences Division, Environmental Sciences Department, Brookhaven National Laboratory, Upton, NY 11973-5000.
[3] Department of Marine, Earth and Atmospheric Sciences, North Carolina State University, Raleigh, NC 27695-8208.
[4] Atmospheric Sciences Division, NASA Langley Research Center, Hampton, VA 23681-0001.

Research by BNL investigators was performed under the auspices of the U.S. Department of Energy under Contract No. DE-AC02-98CH10886.

PERGAMON

Aerosol Science 33 (2002) 319–337

Journal of
Aerosol Science

www.elsevier.com/locate/jaerosci

Retrieval of aerosol properties from moments of the particle size distribution for kernels involving the step function: cloud droplet activation

D.L. Wright[a,*], Shaocai Yu[a], P.S. Kasibhatla[a], R. McGraw[b], S.E. Schwartz[b], V.K. Saxena[c], G.K. Yue[d]

[a] *Nicholas School of the Environment, Duke University, Durham, NC 27708, USA*
[b] *Atmospheric Sciences Division, Environmental Sciences Department, Brookhaven National Laboratory, Upton, NY 11973-5000, USA*
[c] *Department of Marine, Earth and Atmospheric Sciences, North Carolina State University, Raleigh, NC 27695-8208, USA*
[d] *Atmospheric Sciences Division, NASA Langley Research Center, Hampton, VA 23681-0001, USA*

Received 6 November 2000; received in revised form 12 July 2001; accepted 13 July 2001

Abstract

Aerosol properties such as the number of particles that activate to form cloud drops and the mass contained within specified size ranges (as in the PM 2.5 and PM 10 regulatory standards) require integration over only part of the full size range of the particle distribution function (PDF) and may be formally expressed as integrals over kernels involving the Heaviside step function. Determination of these properties requires essentially that the size spectrum be partitioned into two (or more) portions, and poses a special challenge for aerosol modeling with the method of moments. To assess the ability of moment-based methods to treat kernels involving step functions, several algorithms for the estimation of aerosol properties associated with cloud activation have been evaluated. For 240 measured continental distributions employed here as test cases, the full size spectrum of the PDF was partitioned into three distinct portions based upon characteristic critical radii for activation in cumulus and stratiform clouds, and mass- and number-concentration metrics were evaluated for each portion. The first six radial moments yielded results accurate to within about 10% or better, on average, and the numbers of particles activated as cloud drops and the aerosol mass taken into cloud water were estimated to an accuracy of 5% or better. Of the moment-based approaches evaluated, the multiple isomomental distribution aerosol surrogate (MIDAS) (Wright, J. Aerosol Sci. 31 (2000) 1) technique performed best. Accurate results were also

* Corresponding author at: 2005 Westfield Ave, 1st floor, Scotch Plains, NJ 07076, USA.
E-mail address: dlw@bnl.gov (D.L. Wright).

0021-8502/01/$ - see front matter. Published by Elsevier Science Ltd.
PII: S0021-8502(01)00172-0

obtained with the randomized minimization search technique (RMST) (Yue et al., Geophys. Res. Lett. 24 (1997) 651; Heintzenberg et al., Appl. Opt. 20 (1981) 1308). Published by Elsevier Science Ltd.

Keywords: Moments; Modeling; Cloud activation

1. Introduction

There are important aerosol properties requiring integration over part of the size spectrum of the particle distribution function (PDF). Mathematically, these properties can be expressed using kernels involving the Heaviside step function:

$$\theta(x-a)=\begin{cases}1, & x \geqslant a,\\ 0, & x < a.\end{cases}$$

For example, a step function arises with the PM 2.5 and PM 10 air-quality standards, where the aerosol mass loadings must be determined for particles having diameters less than or equal to 2.5 and 10 μm, respectively. Conventionally, the mass (M) per unit volume contained in particles having radii less than or equal to R is represented as

$$M(r \leqslant R)=\frac{4\pi d}{3}\int_0^R r^3 f(r)\,\mathrm{d}r, \tag{1a}$$

where d is the density of the aerosol (assumed for simplicity to be size-independent in this example), and $f(r)$ is the PDF, which gives the number of particles per unit volume within the radius range r to $r+\mathrm{d}r$. Using the Heaviside function, the expression is

$$M(r \leqslant R)=\frac{4\pi d}{3}\int_0^\infty \theta(R-r)r^3 f(r)\,\mathrm{d}r. \tag{1b}$$

The latter form explicitly expresses $M(r \leqslant R)$ as an integral over the entire PDF.

Another example is that of cloud droplet activation for a specified supersaturation, where only those aerosol particles having radius greater than (or equal to) a critical radius (r_c), which depends on supersaturation, activate to form cloud drops. The number of cloud drops per unit volume (N_c) formed upon activation is conventionally expressed as

$$N_c=\int_{r_c}^\infty f(r)\,\mathrm{d}r \tag{2a}$$

and with the Heaviside function

$$N_c=\int_0^\infty \theta(r-r_c)f(r)\,\mathrm{d}r. \tag{2b}$$

In a real cloud, such factors as variable updraft velocities in different air parcels, differing particle compositions, and other heterogeneities will all act, on average, to smooth the step discontinuity in the kernel to a more manageable continuous form. Nevertheless, the Heaviside function has validity for modeling cloud activation in box models when the seed particles are of uniform composition, as is done here, and in any event represents the extreme case that is expected to be the greatest challenge for cloud activation modeling with the method of moments.

Step function kernels also arise during the comparison of measurements of particle number using size-restricted instrumentation with values of particle number computed from models employing moment-based surrogates to the PDF (see below). To permit comparison of modeled particle number counts with measured values from optical particle counters and condensation-type detectors over their respective sensitivity ranges, moment-based surrogates to the PDF must be integrated only over a portion of the full size spectrum of the PDF obtained with the use of such instruments. In such cases, the number of particles (N) per unit volume in the radius range $R_1 \leqslant r \leqslant R_2$ is conventionally expressed as

$$N = \int_{R_1}^{R_2} f(r)\,\mathrm{d}r. \tag{3a}$$

Alternately, such an expression may be written in terms of two step functions in the Heaviside notation:

$$N = \int_0^{\infty} \theta(r - R_1)\theta(R_2 - r) f(r)\,\mathrm{d}r. \tag{3b}$$

The foregoing examples show that Heaviside step functions can generate three distinct types of regions of (non-zero) integration: (1) regions with right-side steps (e.g., PM 2.5/10 standards), (2) regions with left-side steps (e.g., number of cloud drops activated) and (3) regions with steps at both ends of the integration (e.g., comparisons with particle-counter measurements). In this work, moment-based methods will be evaluated for determination of aerosol properties (such as those cited above) for all three types of regions.

1.1. Moments and aerosol properties

The kth radial moment radial is defined as

$$\mu_k = \int_0^{\infty} r^k f(r)\,\mathrm{d}r. \tag{4}$$

It is assumed that only the low-order ($k = 0$–5) moments are known, and the underlying PDF is unknown. Aerosol properties (Φ) can be derived from the moments by quadrature methods as

$$\Phi = \sum_i \varphi(r_i) w_i, \tag{5}$$

where the sum is taken at radii r_i with weights w_i, and where both the r_i and w_i can be determined from the moments alone. Alternatively, more accurate methods for determining

aerosol properties from the moments employ integrals of the form

$$\Phi = \int \varphi(r) g(r)\, \mathrm{d}r, \tag{6}$$

where $g(r)$ is a surrogate for the true PDF derived from the low-order moments. From three moments, the parameters of a single-mode lognormal distribution can be derived, but surrogates obtained from longer moment sequences can be expected to yield more accurate results (Yue et al., 1997). The present study shows that this result holds also for integrals involving Heaviside-type kernels.

Several recent studies have addressed the retrieval of aerosol optical properties from moment sequences, these properties involving the full spectrum of particle size. Optical properties have been computed from the first six radial moments using 3-point quadrature [Eq. (5)] (McGraw, Huang, & Schwartz, 1995), the randomized minimization search technique (RMST) (Yue et al., 1997) and by the multiple isomomental distribution aerosol surrogate (MIDAS) method (Wright, 2000). The latter two methods derive surrogates $g(r)$ to the unknown PDF for use in Eq. (6), and are especially valuable when the quadrature approximation suffers from inadequate sampling of the kernels evaluated. Accuracy is typically within 1–2% when compared to the values of the same optical properties computed directly from the PDF.

1.2. Scope of this study

This work extends previous studies investigating the retrieval of aerosol properties from moment sequences to cases in which the properties of interest are determined from the size distribution by integrations over only part of the full size spectrum.

For properties involving step-function kernels, the computational task requires partitioning the aerosol into two (or more) portions based upon some pre-determined particle size(s). With a moment-based approach for retrieving aerosol properties from moments, portion i of the underlying PDF will then be characterized by its own moment set $\{\mu_k^i\}$ such that $\Sigma_{i\mu_k}^i = \mu_k$.

This partitioning is an especially challenging task for the method of moments (MOM), as the (standard) moments defined in Eq. (4) are integrals over the entire size spectrum of the PDF, and as such do not contain information about specific portions of the PDF. From another point of view, it is known that the MOM works well for polynomial kernels, even yielding the exact results, depending on the degree of the polynomial and the number of moments used in the evaluation (McGraw et al., 1995). Also, the use of surrogates for the PDF derived from the moments has substantially improved the accuracy of integrals even over much more complex functions, albeit in work thus far, functions that are analytical and more or less well behaved (Yue et al., 1997; Wright, 2000). The Heaviside function, however, is markedly not of polynomial form and is not even analytical.

Even though these considerations may seem at first to preclude the use of the MOM for such applications, there are reasons for anticipating that a moment-based approach will have some degree of success. Although the algorithms evaluated in this work for partitioning the PDF require only a sequence of moments as input, most contain implicit assumptions about the PDF: that it is positive-definite, that it typically has internal (rather than endpoint) maxima, and some degree of smoothness. That these assumptions are reasonable for aerosol size distributions, and

are utilized in deriving surrogates to the PDF from its moments, probably accounts for much of the previous success of techniques for retrieving aerosol properties from moments, and offers hope for success in evaluating integrals over such extremely non-polynomial kernels as those involving the step function.

In anticipation of developing a moment-based module for use in CTMs that includes representation of aerosol evolution in clouds (Wright, Kasibhatla, McGraw, & Schwartz, 2001), this study explores moment-based algorithms for partitioning the size spectrum of the PDF in the context of cloud droplet activation. For 240 measured continental distributions employed here as test cases, the full size spectrum of the PDF was partitioned into three distinct portions based upon characteristic critical radii for activation in cumulus and stratiform clouds, and mass- and number-concentration metrics were evaluated for each portion. The results presented here should provide reliable indications of the performance of these moment-based methods in the evaluation of other aerosol properties involving step-function kernels. With appropriate rescaling of the test distributions and the assumed critical radii for cloud activation, the test distributions and the radii at which the step function yields an on–off switch could be brought close to those appropriate for evaluations in the context of the PM 2.5 and PM 10 mass concentration standards noted above.

In this investigation, for 240 measured continental distributions employed here as test cases, the full size spectrum of the PDF was partitioned into three distinct portions based upon characteristic critical radii for activation in cumulus and stratiform clouds. Mass- and number-concentration metrics were then evaluated for each portion in order to assess the accuracy and computational requirements of several moment-based algorithms for partitioning the size-spectrum of the PDF. This assessment focuses on the RMST and MIDAS methods, although a few simpler approaches using fewer than six moments are also examined, mainly as points of comparison for the techniques based on six moments. Metrics computed using the moment-based approaches are evaluated by comparison with benchmark values computed by direct integration over the 240 test distributions.

In Section 2 we describe the moment-based approaches to be investigated. In Section 3 we describe the test distributions and define the metrics to be evaluated. In Section 4 we present the results and discuss the sensitivities of the RMST and MIDAS performances to various parameters in these algorithms. In Section 5 we summarize the findings of this study.

2. Description of methods

The methods for evaluating integrals of a kernel function over a PDF using only the moments of the distribution consist of taking integrals over surrogate distributions that are derived from the moments. Here we briefly describe the types of surrogates investigated in this study.

2.1. 1-Modified gamma

This is a simple 2-moment approach. The modified gamma distribution is the surrogate

$$g(r) = f_{\mathrm{MG}}(r) = \frac{Nsb^{(n-1)/s} r^n}{\Gamma[(n+1)/s]} \exp(-br^s), \tag{7}$$

where N is the number of particles. The parameters n and s are set to unity, permitting evaluation of aerosol properties via Eq. (6) by analytical integration of the required kernels and the avoidance of computationally expensive numerical integration. The volume moment was used to determine b through $\mu_3 = 24N/b^3$ with $N = \mu_0$.

2.2. 1-Lognormal

This is a simple 3-moment approach. The lognormal distribution is the surrogate

$$g(r) = f_{\mathrm{LN}}(r) = \frac{N}{r\ln(\sigma)\sqrt{2\pi}} \exp\left\{-\frac{1}{2}[\ln(r/R_{\mathrm{g}})/\ln(\sigma)]^2\right\}, \tag{8}$$

where N, R_{g}, and σ are the number of particles, geometric mean radius, and geometric standard deviation, respectively. These parameters are determined algebraically from μ_0, μ_3 and μ_5. Numerical integration is required to obtain aerosol properties from Eq. (6).

2.3. 3-Point quadrature

For the evaluation of integral aerosol properties using quadrature, an N-point Gaussian quadrature (with unknown weight functions) using the lowest $2N$ moments yields N abscissas (particle radii) and N weights (particle numbers), which may be considered an N-disperse surrogate for the unknown PDF. The routine ORTHOG of Press, Teukolsky, Vetterling, and Flannery (1992) efficiently yields the N abscissas and weights from the moments. These quadrature points yield rapid estimates of aerosol properties, and this approach has been evaluated for the computation of aerosol optical properties, as previously described. Here we use six moments and obtain three quadrature points from which the required integrations are obtained from Eq. (5).

2.4. Multiple isomomental distribution aerosol surrogate (MIDAS)

The MIDAS technique is presented in Wright (2000). MIDAS retrieves smooth multi-modal surrogates to the unknown PDF, which are composed of lognormal or modified-gamma distributions. The final surrogate PDF will have M modes, for $M/3$ retrievals of trimodal distributions. Desired aerosol properties are then obtained by numerical integration over the distribution surrogates using Eq. (6). The QSIMP routine of *Numerical Recipes* (Press et al., 1992) was used for the numerical integrations, where the degree of convergence was regulated using the parameter EPS, discussed below.

2.5. Randomized minimization search technique (RMST)

A detailed description of the RMST method may be found in Heintzenberg, Muller, Quenzel, and Thomalla (1981), Lin and Saxena (1992), and Saxena, Anderson, and Lin (1995), and its extension to moments in Yue et al. (1997). The RMST approach obtains a bin-section type surrogate to the PDF. In the moment-based applications contemplated here, the size range of the underlying distribution will not be precisely known, and the bin structure must be determined with the aid of the moments themselves. In this work, the mean radius of each moment set

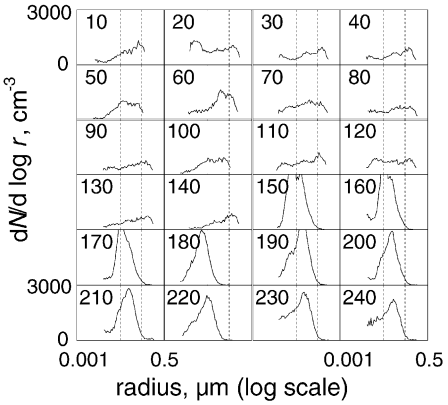

Fig. 1. Twenty-four of the 240 (dry) test distributions derived from DMPS measurements plotted as equal-area plots, $dN/d\log_{10}(r)$ vs. r. Dotted vertical lines are drawn at $r_1 = 0.022$ μm and $r_2 = 0.10$ μm to indicate the partitioning of the distributions into three portions.

($R_{mean} = \mu_1/\mu_0$) was used to set the first and last bin radii according to $r_1 = 0.06R_{mean}$ and $r_L = 6.0R_{mean}$, with the number of bins then determining all bin radii between these limits, which are geometrically spaced. For each specified set of moments, several retrievals are done, and averaging over all retrieved distributions further smoothes the final surrogate, from which aerosol properties are computed using Eq. (6).

3. Test distributions and metrics

3.1. Test distributions

The aerosol size distributions used as test cases were derived from field observations with a differential mobility particle sizer (DMPS) at ambient relative humidity (RH) on Black Mountain, North Carolina (Wenny et al., 1998; Yu et al., 2000). The measurements yielded number of particles as a function of radius for radii ranging from 0.008 to 0.3 μm (at ambient RH), in 50 size-bins. Size distributions were measured every 15 min and relative humidity was measured every hour during the daytime. The selected dataset is comprised of 240 distributions from six days of measurements, with the first 142 distributions measured in August 1995, and the remainder measured in September 1995. For this methodological study, the measured ambient size distributions were converted to dry distributions using the measured RH. For this conversion, the solute was taken to be pure ammonium sulfate, and the data of Tang and Munkelwitz (1994) were used to obtain the ratio of ambient ("wet") particle radius to dry radius; here, dry radius is the radius of the sphere of equal volume. This ratio was taken as dependent on RH but independent of particle size; thus the small reduction in water uptake at the smallest particle sizes due to the Kelvin effect was neglected. The moments of the dry distributions were calculated for input to the moment-based methods.

Fig. 1 shows selected (dry) test distributions as equal-area plots, $dN/d\log_{10}(r)$ vs. r. Due to the instrumental detection limits, the measured distributions do not always include the full

ambient size spectrum, with the result that some of the observed shapes are truncated and therefore are not physically realistic or characteristic of those that arise in aerosol modeling. Those cases in which detection limits play a role in shaping the test PDFs are likely to be more difficult to treat as the abrupt onset or termination of the PDF with particle size is not easily captured by a modal approach to the surrogate, or by a bin-sectional approach when the precise range of particles sizes is not specified. In the case of modeling with the MOM, the full size spectrum of the underlying PDF is implicitly present as there are no a priori restrictions on particle size and growth. The selected cases encompass a wide range of distributions and provide a relatively comprehensive dataset for method evaluation.

3.2. Metrics

For the purpose of these evaluations, cumulus and stratiform cloud types were assigned characteristic peak supersaturations of 0.5% (cumulus) and 0.05% (stratiform) (Seinfeld & Pandis, 1998). The minimum particle dry radius that can activate was estimated using $r_{\mathrm{dry,min}}(\mu\mathrm{m}) = 1.40 \times 10^{-2} S^{-2/3}$ (Gong, Barrie, & Blanchet, 1997; Schwartz, 1996) where S is the supersaturation (in percent), yielding $r_{\mathrm{dry,min}}$ values of $r_1 = 0.022$ and $r_2 = 0.10\ \mu\mathrm{m}$ for cumulus and stratiform clouds, respectively. These two particle radii were used to partition the PDF into three portions: $r \leqslant r_1$, $r_1 < r \leqslant r_2$, and $r > r_2$. This partitioning is indicated with dashed vertical lines in Fig. 1.

To evaluate and compare the several moment-based approaches, we defined several metrics. Specifically, metrics M_1, M_2, and M_3 are defined as the aerosol solute mass concentrations in portions 1, 2 and 3, respectively, and metrics N_1, N_2, N_3 are defined as the aerosol particle number concentrations in portions 1, 2 and 3, respectively:

$$M_1 = \frac{4\pi d}{3} \int_0^{r_1} r^3 f(r)\,\mathrm{d}r = \frac{4\pi d}{3} \int_0^{\infty} \theta(r_1 - r) r^3 f(r)\,\mathrm{d}r, \tag{9a}$$

$$M_2 = \frac{4\pi d}{3} \int_{r_1}^{r_2} r^3 f(r)\,\mathrm{d}r = \frac{4\pi d}{3} \int_0^{\infty} \theta(r - r_1)\theta(r_2 - r) r^3 f(r)\,\mathrm{d}r, \tag{9b}$$

$$M_3 = \frac{4\pi d}{3} \int_{r_2}^{\infty} r^3 f(r)\,\mathrm{d}r = \frac{4\pi d}{3} \int_0^{\infty} \theta(r - r_2) r^3 f(r)\,\mathrm{d}r, \tag{9c}$$

$$N_1 = \int_0^{r_1} f(r)\,\mathrm{d}r = \int_0^{\infty} \theta(r_1 - r) f(r)\,\mathrm{d}r, \tag{9d}$$

$$N_2 = \int_{r_1}^{r_2} f(r)\,\mathrm{d}r = \int_0^{\infty} \theta(r - r_1)\theta(r_2 - r) f(r)\,\mathrm{d}r, \tag{9e}$$

$$N_3 = \int_{r_2}^{\infty} f(r)\,\mathrm{d}r = \int_0^{\infty} \theta(r - r_2) f(r)\,\mathrm{d}r, \tag{9f}$$

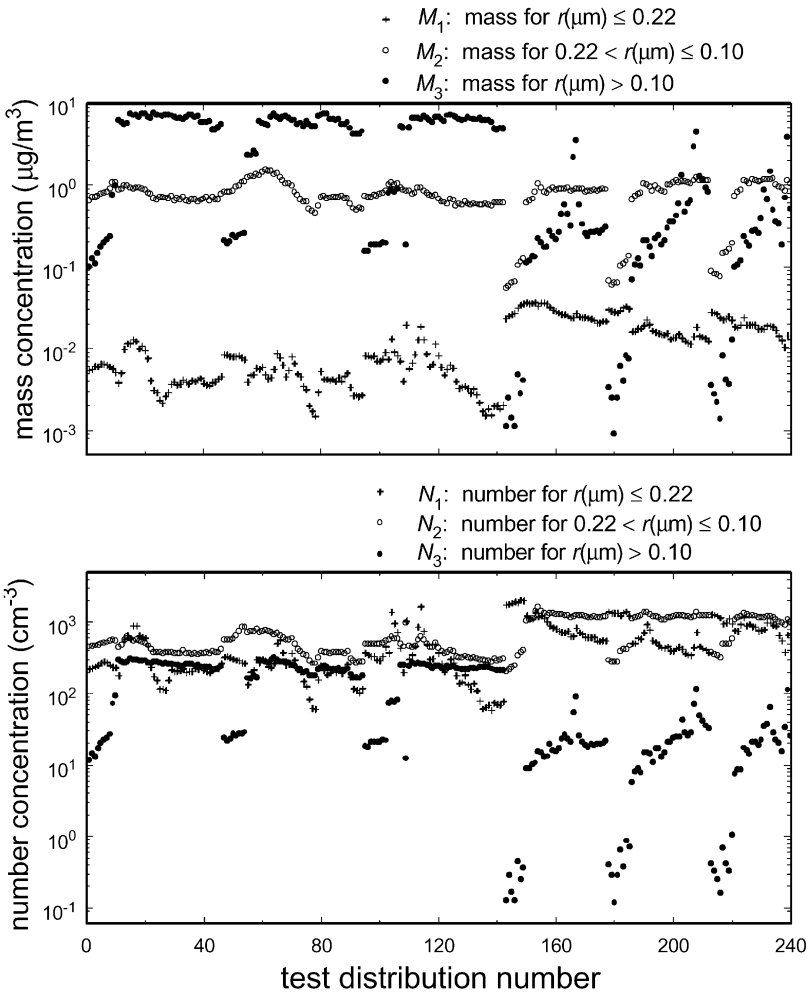

Fig. 2. (a) Metrics M_1, M_2 and M_3 obtained directly from the test distributions as a function of test distribution number, used as benchmarks to evaluate the moment-based approaches. These metrics are based on aerosol mass concentrations. (b) Metrics N_1, N_2 and N_3 obtained directly from the test distributions as a function of test distribution number, used as benchmarks to evaluate the moment-based approaches. These metrics are based on aerosol number concentrations.

where d is the density of dry ammonium sulfate (1.77×10^{-12} g/μm^3), and r the radius of the equivalent sphere. We examined both the accuracy and computational expense of each moment-based method for computing these integrals. For comparisons of efficiency, the CPU time required for each method to compute the six integrals for all 240 test distributions from their moments was obtained on the same Sun Spark Enterprise.

Fig. 2 shows the values of the metrics obtained from each test distribution. Mass concentrations in the three portions of the size spectrum (M_1, M_2, M_3) range from about 10^{-15} to 10^{-11} g/cm^3; number concentrations (N_1, N_2, N_3) range from about 0.01 to 2000 cm^{-3}. A few of the test cases have very little aerosol present.

4. Results

4.1. Overall performance of the moment-based approaches

The percent error in a metric for a moment-based method is defined as $\%e(P_i) = \{100\% \times [P_i(\text{moment-based}) - P_i(\text{exact})]/P_i(\text{exact})\}$, where P_i is either M_i or N_i. We summarize the performance of each method by computing the average magnitude of percent error, defined as

$$\langle \%e(P_i) \rangle = (1/N_d)\Sigma_n[|\%e(P_i)|]_n \tag{10}$$

for the $N_d = 240$ test distributions. Here and throughout the rest of the paper we use the term "average percent error" to refer to the average of the magnitude (absolute value) of the percent error; averaging the magnitude of the percent error provides a better test of accuracy as it does not allow for compensating positive and negative errors.

Although a moment-derived surrogate to a PDF may be expected to provide a good representation of its key attributes—its integral, mean value, width—it cannot be expected to closely match the amplitude of the PDF at each point along the size spectrum. Specifically, as the region of (non-zero) integration narrows (for example for integration from a Heaviside "step" at radius R to infinity is done, and R is moved out to larger and larger radius and onto the tail of the PDF), the fraction of the total aerosol present in that region is reduced. As the moment-derived surrogate may not match the actual PDF amplitude in this (or any other) small region, one would expect, on the whole, for the relative errors to increase as the fraction of the PDF included in the range of integration is reduced. Larger errors in the metrics will thus tend to be correlated with integrations over regions containing a small fraction of the total particle number, and thus tend to be correlated with small values of those metrics. This will be discussed later in Section 4.4. To examine this expectation, and to better assess the overall performance of the moment-based algorithms, we also evaluate the metric-weighted average magnitude of percent error, defined as

$$\langle \%e(P_i) \rangle_W = \Sigma_n[|\%e(P_i)|P_i]_n/\Sigma_n[P_i]_n \tag{11}$$

over the N_d test distributions.

The results shown in Tables 1 and 2 are taken from 36 evaluations of these errors in the metrics for several variants of the moment-based algorithms described above. The metric-weighted average errors are, as anticipated, almost always smaller than the corresponding unweighted average errors, indicating that larger errors tend to be associated with smaller values of the metrics, which often correspond in our dataset to insignificant aerosol concentrations. We take the metric-weighted average errors as most representative of the errors to be expected when significant amounts of aerosol are present.

It can be seen (from Evaluation 6; MIDAS with 12 modified-gamma modes) that on average mass and number concentrations in each of these portions of the size spectrum are estimated to within 3–13% using a moment-based approach. The number concentration that activates to form cloud drops in stratiform clouds (N_3) is estimated on average to within about 5%. The number concentration that does not activate to form cloud drops in cumulus clouds (N_1), and thus remains as interstitial aerosol, is also estimated on average to within 5% (Evaluation 6).

Table 1
Average magnitude of percent error and metric-weighted average magnitude of percent errors for metrics M_1, M_2, and M_3, the mass concentrations in portions $r \leqslant 0.022$ μm, 0.022 μm $< r \leqslant 0.10$ μm, and $r > 0.10$ μm, respectively, for the moment-based techniques[a]

		Unweighted			Metric-weighted			
No.	Description	M_1	M_2	M_3	M_1	M_2	M_3	CPU (s)
1	1-MG	57.6	62.1	14.5	30.7	61.1	15.6	0.13
2	1-LN	19.6	29.3	28.3	18.7	29.1	7.4	0.84
MIDAS								
3	MIDAS-3MG	42.1	8.5	13.9	13.8	21.7	3.7	10.26
4	MIDAS-6MG	36.0	8.3	12.7	12.5	19.3	3.3	18.77
5	MIDAS-12MG-*a*	20.5	9.6	8.3	13.4	10.1	2.6	36.24
6	MIDAS-12MG-*c*	20.5	9.7	8.4	13.4	10.1	2.6	15.14
7	MIDAS-12LN-*c*	36.3	10.3	9.9	19.2	12.1	3.1	5.95
RMST								
8	RMST-10-5-1	19.7	9.9	12.5	15.8	10.8	3.0	23.48
9	RMST-20-5-1	20.1	15.0	14.1	13.6	15.1	3.8	77.82
10	RMST-20-1-1	30.6	17.4	15.3	22.4	17.7	4.6	17.23
11	RMST-20-10-1	16.8	14.1	14.2	11.6	14.0	3.6	155.38
12	RMST-20-20-1	14.8	14.7	14.1	10.7	14.7	3.7	297.44

[a]For the MIDAS results, MG indicates modified gammas, LN lognormals; $3, 6, 12$ indicates the number of modes averaged to form the final surrogates, and a, b, c indicate convergence requirements in the numerical integration (Section 4.2). For the RMST results, the numbers X–Y–Z indicate the number of bins, the number of solutions averaged to form the final surrogates, and the convergence tolerance (%) during the retrieval process (Section 4.3), respectively.

Evaluations 1 and 2 summarize results with the 1-modified gamma and 1-lognormal approaches. Although these simpler methods required significantly less CPU time than the other algorithms, they were markedly less accurate. This decrease in accuracy illustrates the importance of utilizing all six moments (when available) for computing these aerosol properties. The errors obtained with the more general 3-point quadrature (not shown here) were almost always the largest of the methods evaluated in this work, illustrating the limitations of 3-point Gaussian quadrature for evaluated step-function kernels. If extremely rapid estimates are essential, RMST or MIDAS can deliver more accurate results than these simpler techniques in nearly comparable CPU time with the appropriate choice of algorithm parameters.

4.2. Sensitivity study for MIDAS

Evaluations 3–7 in Table 1 show part of a sensitivity study for the MIDAS method. We have explored the sensitivity of the MIDAS metrics to: (1) the number of retrievals averaged to form the distribution surrogates ($M/3$ in Section 2.3), and (2) the accuracy demanded in numerical integrations over the surrogates in evaluating the metrics.

Table 2
Average magnitude of percent error and metric-weighted average magnitude of percent error for metrics N_1, N_2, and N_3, the number concentrations in portions $r \leqslant 0.022$ μm, 0.022 μm $< r \leqslant 0.10$ μm, and $r > 0.10$ μm, respectively, for the moment-based techniques[a]

		Unweighted			Metric-weighted		
No.	Description	N_1	N_2	N_3	N_1	N_2	N_3
1	1-MG	62.7	37.5	17.0	39.4	30.5	10.1
2	1-LN	29.6	24.7	29.1	22.5	20.1	19.0
MIDAS							
3	MIDAS-3MG	18.6	13.9	7.4	9.1	11.3	8.3
4	MIDAS-6MG	12.7	12.6	5.4	6.4	8.2	6.9
5	MIDAS-12MG-*a*	7.8	4.1	11.1	5.1	3.5	5.0
6	MIDAS-12MG-*c*	7.9	4.3	11.2	5.1	3.6	5.3
7	MIDAS-12LN-*c*	14.6	6.3	16.7	8.2	5.6	9.8
RMST							
8	RMST-10-5-1	18.1	12.0	21.7	9.0	8.7	15.7
9	RMST-20-5-1	15.0	12.2	25.6	8.1	8.7	20.3
10	RMST-20-1-1	22.3	15.1	27.1	13.1	12.0	19.4
11	RMST-20-10-1	14.5	11.7	25.3	7.5	8.2	19.4
12	RMST-20-20-1	13.8	11.7	25.7	7.3	8.3	20.3

[a]Notation is the same as in Table 1.

Evaluations 3–5 show that the MIDAS results do improve as the number of retrievals is increased from 1 to 4, but also that the time required to compute these metrics is essentially proportional to M.

To examine the sensitivity of the MIDAS CPU time to the convergence required of the numerical integrations over the surrogates, integrations were done with convergence tolerances (the parameter EPS in the QSIMP routine) set to 0.0001, 0.001 and 0.005, with the results using $\mathrm{EPS} = (0.0001, 0.005)$ indicated as $(-a, -c)$ in Tables 1 and 2. Increasing EPS from 0.0001 to 0.001 resulted no significant change in the error statistics, and increasing EPS to 0.005 gave little change.

On the basis of these sensitivity analyses, it would appear that the 12-mode modified gamma version of MIDAS (Evaluation 6) best represents the capabilities of this technique for these applications.

4.3. Sensitivity study for RMST

Evaluations 8–12 show part of a sensitivity study for RMST, where the bin structure, number of bins, number of solutions, and convergence tolerance are the most important parameters. The sensitivity of the RMST results to: (1) the number of bins, (2) the number of solutions averaged, and (3) the convergence tolerance was explored.

Increasing the number of bins does not necessarily result in increased accuracy of the computed metrics, as can be seen from comparison of Evaluations 8 and 9. The surrogates can

become "noisy" (strong bin-to-bin variation) if too many bins are used, and the loss of smoothness probably tends to decrease accuracy.

Increasing the number of solutions used to form the final surrogates would be expected to increase accuracy, as is borne out by comparison of Evaluations 10–12, where the number of solutions is set at 1, 10 and 20, respectively. Increasing the number of solutions from 1 to 10 resulted in increased accuracy, but there was almost no further improvement when going on to 20 solutions. As CPU time is nearly proportional to the number of solutions obtained, 10 solutions or less is probably a good choice.

Increasing the convergence tolerance used to obtain each solution, thereby decreasing solution accuracy, has a slight impact on accuracy but a large impact on the CPU time required. If the accuracy is too low, numerical problems can potentially arise in the context of the method-of-moments algorithm in which this method would be embedded, so a tolerance of 1% is perhaps a good choice.

On the basis of this sensitivity analysis, results using perhaps 10 bins, 5 solutions, and 1% convergence tolerance appear to be representative of the capabilities of RMST for applications such as those contemplated here.

4.4. Comparison of representative MIDAS and RMST results

Evaluations 6 and 8 were selected for more detailed comparison of these algorithms. For the MIDAS results with 12 modified-gamma modes and EPS = 0.005 (MIDAS-12MG-c), the metric-weighted average errors for M_1, M_2, M_3, N_1, N_2, N_3 were 13.4%, 10.1%, 2.6%, 5.1%, 3.6%, 5.3% and the computations required 15.14 CPU s. For the RMST results with 10 bins, 5 solutions and 1% convergence tolerance (RMST-10-5-1) those errors were 15.8%, 10.8%, 3.0%, 9.0%, 8.7%, 15.7% and the required CPU time was 23.48 s.

The overall performance of these two algorithms is similar for distributions 143–240 (September field data), whereas MIDAS performs better for distributions 1–142 (August field data). Both methods perform better for the September distributions, as both capture the PDF shape quite well during this period (see Sections 4.5 below regarding distribution 169). The better performance on metrics M_1, M_2, N_1, and N_2 of both RMST and MIDAS for distributions 143–240 compared to that for distributions 1–142 is associated with the larger metrics values for the September distributions. This association is also apparent when the metric-weighted and unweighted average errors are compared.

Fig. 3 shows the errors in the MIDAS-12MG-c and RMST-10-5-1 metrics M_3 and N_3 as a function of test distribution number, and shows a daily periodicity in the errors in these metrics for the September distributions for both algorithms. There are three data subsets, consisting of distributions 143–177 (September 3), distributions 178–212 (September 4), and distributions 213–240 (September 5), and the errors in these metrics within each subset tend to vary roughly from their most negative to their most positive values over the course of each day. This can most immediately be correlated with a slow shift in the location of the PDF from smaller to larger dry radius over the course of each of these days, observable in Fig. 1. These daily shifts in the PDFs correspond to daily variations in relative humidity, as the distributions used in this study were measured at ambient RH, but the distributions used in the calculations correspond to a dry aerosol; the particle radii were decreased from

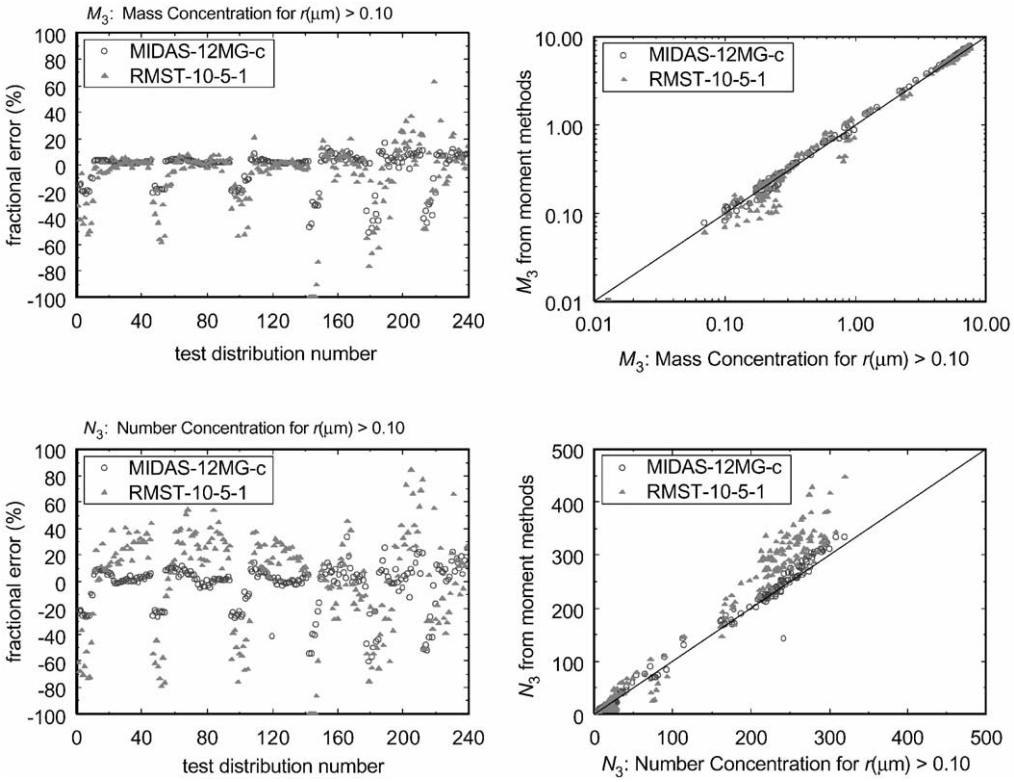

Fig. 3. Left panels: Percent errors in the mass (M_3) and number (N_3) concentration metrics for the size range $r > 0.10$ μm for MIDAS-12MG-*c* and RMST-10-5-1, as a function of test distribution number. Right panels: Metrics M_3 and N_3 from MIDAS-12MG-*c* and RMST-10-5-1 plotted against those metrics computed directly from the test distributions.

the measured values to those for a dry aerosol, for an assumed RH dependence equal to that of ammonium sulfate. The ambient RH on each of these days began with a high ($\approx$ 100%) value at the beginning of each day and decreased throughout the remainder of the day. Thus the water uptake ratio used to scale ambient particle radius to dry radius was at its maximum at the beginning of each daily subset, and thus the earlier distributions in each day were shifted to smaller dry radii to a greater degree than the distributions measured later in the day. These metrics (M_3 and N_3) showing daily periodicity are derived from the portion of the PDFs at $r > 0.10$ μm, and when the ambient PDFs are dried according to high RH values, often an especially small portion of the PDF extends into this size range. [The RMST errors in metrics M_3 and N_3—100% for distributions 143–146 resulted from the fact that none of the RMST bins remained within this right-hand portion after drying the aerosol; this can be remedied by enlarging the size-spectrum spanned by the bin structure.] A small fraction of the PDF being present in the region of integration results both in small values for these quantities, and in greater errors in moment-derived estimates, as it is unlikely that moment-derived surrogates will accurately match the PDF over such a small portion of the PDF, as discussed above. As explored further below, some of the largest errors for both algorithms are associated with very

small values of the metrics, as can be seen by comparison of the errors with the metrics in Fig. 2, and as are reflected in the differences in the metric-weighted and unweighted average errors.

Also shown in Fig. 3 are the MIDAS-12MG-*c* and RMST-10-5-1 values of M_3 and N_3 plotted against those metrics computed directly from the test distributions. Both methods (and especially RMST) overestimate N_3 when its value exceeds 150 cm^{-3} and a larger fraction of the total particle number has $r > 0.10$ μm. Most of this overestimation occurs at particle sizes just greater than $r = 0.10$ μm (see the MIDAS and RMST surrogates discussed in Section 4.5 below) and is therefore less important for mass (M_3), mass being dominated by the largest particles. This accounts for the fact that on the whole mass is not overestimated for $r > 0.10$ μm by these methods.

To further investigate the association of large errors in moment-derived metrics with small metric values, Fig. 4 shows percent errors in the mass concentration metrics M_1, M_2, and M_3 as a function of the fractions M_1/M, M_2/M, and M_3/M, respectively, with $M = M_1 + M_2 + M_3$, the total mass concentration over the full size spectrum of the PDF, for the MIDAS-12MG-*c* and RMST-10-5-1 results. Also shown are results for the number concentration metrics N_1, N_2, and N_3 as a function of the fractions N_1/N, N_2/N, and N_3/N, respectively, with $N = N_1 + N_2 + N_3$, the total number concentration over the full size spectrum of the PDF. These results confirm the discussion in Section 4.1 concluding that larger errors in the moment-derived metrics are likely to be associated with smaller fractions of the mass/number concentrations within the regions of integration. As these mass/number fractions tend to unity, the errors in these metrics must tend to zero as integration over the full PDF corresponds to the moments, which are known quantities. These results may be useful in estimation of the accuracy of moment-derived aerosol properties when integration over only a portion of the PDF is required. For example, if one were to compute an aerosol property over half of the PDF; and the property can be computed accurately when the integration is extended over the full PDF, the MIDAS results for both mass- and number-concentrations in this figure suggest that perhaps an accuracy of 10–20% could be expected.

Although not explicitly represented in the metrics of this study, the number of particles that activate as cloud drops and the aerosol mass per unit volume taken into cloud water in cumulus clouds, given by $M_{\text{cumulus}} = M_2 + M_3$ and $N_{\text{cumulus}} = N_2 + N_3$, respectively, are important in the applications of interest in this work. The average errors in M_{cumulus} and N_{cumulus} were 0.18% and 3.6%, respectively, for MIDAS-12MG-*c* and 0.35% and 5.3%, respectively, for RMST-10-5-1. These mass-concentration errors are especially small as almost all of the aerosol mass is contained in particles with $r > 0.022$ μm, the portion of the distribution assumed in this study to activate in cumulus clouds, and hence the moment-based integrations are quite accurate.

4.5. Moment-derived surrogates for selected test distributions

A few test distributions were selected for examination for which all moment-based algorithms performed relatively poorly on at least one metric (No. 11, 16, 26, 36, 55, 57, 61, 91, 113, 119, 135) and one test distribution for which most algorithms performed well (No. 169). These distributions are plotted in Fig. 5, along with the MIDAS 12MG-*c* and the RMST-10-5-1

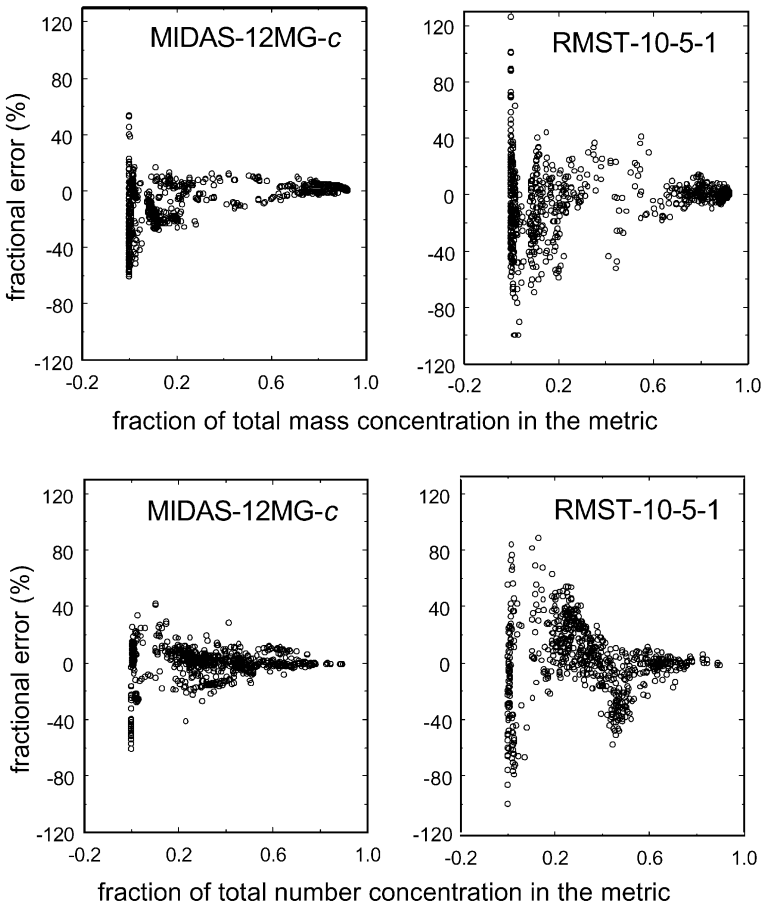

Fig. 4. Upper panels: Percent errors in the mass concentration metrics M_1, M_2, and M_3 as a function of the fractions M_1/M, M_2/M, and M_3/M, respectively, with $M = M_1 + M_2 + M_3$, the total mass concentration over the full size spectrum of the PDF, for the MIDAS-12MG-c and RMST-10-5-1 results. Lower panels: Analogous results for the number concentration metrics N_1, N_2, and N_3 as a function of the fractions N_1/N, N_2/N, and N_3/N, respectively, with $N = N_1 + N_2 + N_3$, the total number concentration over the full size spectrum of the PDF.

surrogates. The close agreement of the actual PDF and its surrogates in distribution 169 is characteristic of the agreement for many of the September distributions.

For distributions 11 and 16 the MIDAS-12MG-c errors in Metric 1 are -36% and -42%, respectively, which can be seen in Fig. 5 to result from a strong dip in the MIDAS surrogate just before the partition at $r = 0.022$ μm, and especially as this is a mass concentration metric and thus derived from the integral over r^3. Similar behavior is also seen in the MIDAS-12MG-c results for Metric 1 for distributions 55, 57 and 61. For distribution 135, this MIDAS variant overestimates Metric 1 by 53%, a result of a component mode in the surrogate peaking just before $r = 0.022$ μm. The lognormal MIDAS surrogates show similar features, with more pronounced multi-modality than with the modified gamma surrogates. These observations seem to be characteristic of those distributions where the MIDAS errors are largest, and illustrate how

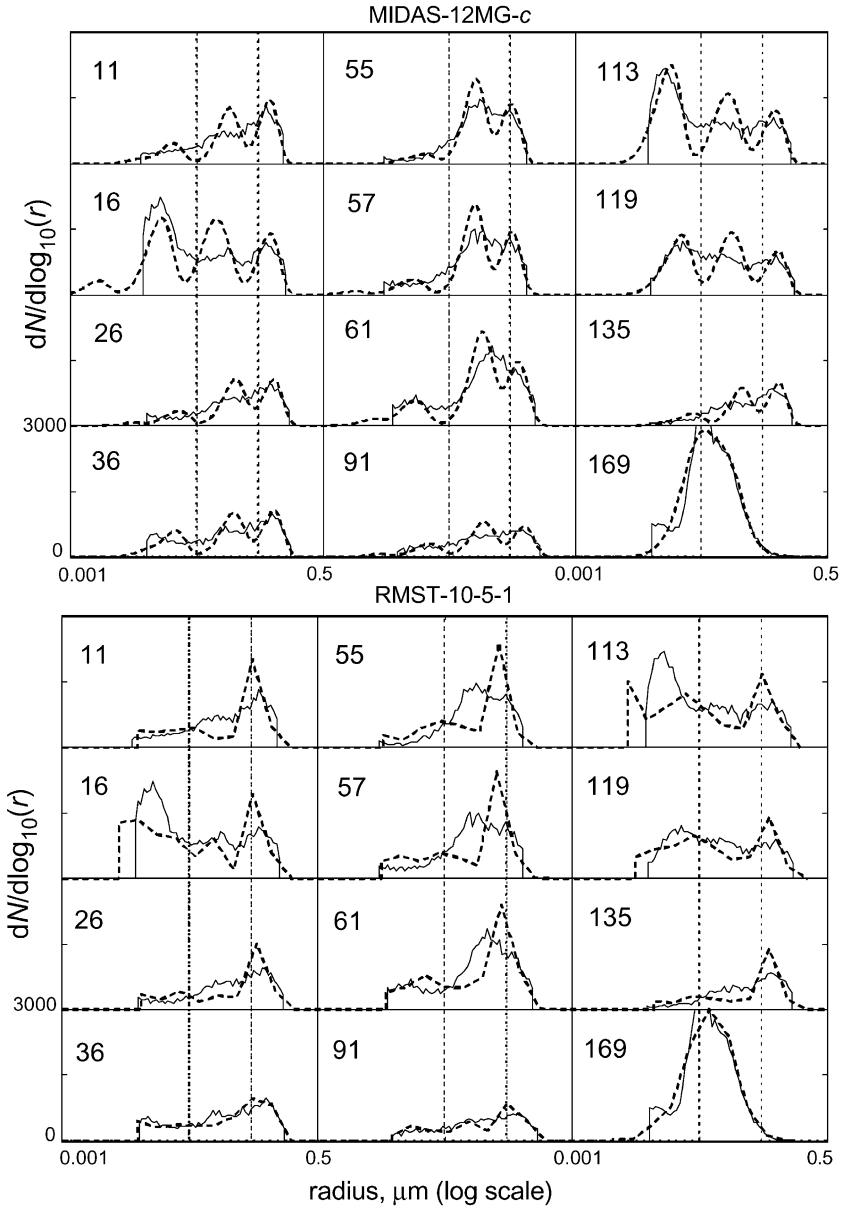

Fig. 5. Retrieved surrogates for the test distributions derived from the moments for 12 selected cases, plotted as equal-area plots, $dN/d\log_{10}(r)$ vs. r. Black lines are the test distributions derived from DMPS measurements, dotted lines the MIDAS 12MG-c and the RMST-10-5-1 surrogates. Dotted vertical lines are drawn at $r_1 = 0.022$ μm and $r_2 = 0.10$ μm to indicate the partitioning of the distributions into three portions.

excessive multi-modality can lead to weaker performance with MIDAS. The MIDAS performance in such cases can be improved by averaging a larger number of retrievals over a wider range of distributions parameters in forming the final surrogate PDF, but with an attendant increase in computational expense.

For the RMST-10-5-1 results shown in Fig. 5, it is more difficult to associate the greater errors (M_1 for distributions 26 and 91 and N_1 for distributions 57 and 135, for example) with specific characteristic features in the RMST surrogates. Despite the overall larger errors in the RMST-10-5-1 metrics compared to those of MIDAS-12MG-c for these distributions, the RMST-10-5-1 surrogates perhaps better capture the shapes of the test distributions than the MIDAS surrogates.

5. Summary and conclusions

We have evaluated several algorithms for computing aerosol properties from moments when the associated kernels involve the step function. Based on these evaluations, moment-based algorithms can be expected to provide estimates of properties such as cloud drop number and the mass loadings associated with size-specific regulatory standards to within about 10% or less, based on the metric-weighted average magnitude of errors shown in Tables 1 and 2. The number of particles activated as cloud drops and the aerosol mass taken into cloud water can be estimated from six moments to within 5% or less for both cumulus and stratiform clouds. The MIDAS technique gave better overall performance than the RMST approach.

The test distributions in this work yielded the exact moments for use by the moment-based methods. In modeling with the method of moments (MOM) however, error will accrue in the moments due to approximations in the dynamics, and this is expected to reduce the accuracy of computed aerosol properties. Wright et al. (2001) evaluates the accuracy of MOM in representing aerosol dynamics, but the impact of these dynamical errors in the moments on aerosol properties has not been explored.

We conclude that the moment-based MIDAS and RMST methods are useful for the computation of aerosol properties even when the properties are derived from only part of the size range of the underlying PDF; the value of these techniques for the determination of aerosol properties derived from the full size spectrum (such as optical properties) has already been established. RMST and MIDAS can now enhance the capabilities of the MOM for representing aerosol evolution in atmospheric models, and the findings of this study have guided the development of algorithms for treating aerosol–cloud interactions in Chemical Transformation Models (Wright et al., 2001). Accurate and compact representations of aerosol evolution and properties based on the MOM are finding increased application, to permit treatment of aerosols limited more by knowledge of the underlying processes rather than by computing resources. This is especially so when external mixtures of several aerosol populations require independent representation.

Acknowledgements

Work done at Duke was supported by Grant NA76GP0350 from NOAA Office of Global Programs, and Subcontract G-35-W62-G2 from Georgia Institute of Technology (Principal Grant R 826372-01-0 from EPA). Work done at BNL was supported in part by NASA through

Interagency Agreement No: W-18,429 as part of its interdisciplinary program on tropospheric aerosols, and in part by the Environmental Sciences Division of the US Department of Energy (DOE) as part of the Atmospheric Chemistry Program, and was performed under the auspices of DOE under Contract No. DE-AC02-98CH10886.

References

Gong, S. L., Barrie, L. A., & Blanchet, J.-P. (1997). Modeling sea salt aerosols in the atmosphere 1. Model development. *Journal of Geophysical Research*, *102*, 3805–3818.

Heintzenberg, J., Muller, H., Quenzel, J., & Thomalla, E. (1981). Information contents of optical data with respect to aerosol properties: Numerical studies with a randomized minimization-search-technique inversion algorithm. *Applied Optics*, *20*, 1308–1315.

Lin, N. H., & Saxena, V. K. (1992). Characteristics of Antarctic stratospheric aerosols during the 1987 ozone depletion episode based on SAGE II satellite observations. *Journal of Geophysical Research*, *97*, 7635–7649.

McGraw, R., Huang, P. I., & Schwartz, S. E. (1995). Optical properties of atmospheric aerosols from moments of the particle size distribution. *Geophysical Research Letters*, *22*, 2929–2932.

Press, W. H., Teukolsky, S. A., Vetterling, W. T., & Flannery, B. P. (1992). *Numerical recipes in FORTRAN*. Cambridge: Cambridge University Press.

Saxena, V. K., Anderson, J., & Lin, N. -H. (1995). Changes in Antarctic stratospheric aerosol characteristics due to volcanic eruption as monitored by SAGE II satellite. *Journal of Geophysical Research*, *100*, 16,735–16,751.

Schwartz, S. E. (1996). Cloud droplet nucleation and its connection to aerosol properties. In M. Kulmala & P. E. Wagner (Eds.), *Nucleation and Atmospheric Aerosols* (pp. 770–779). New York: Elsevier Science Ltd.

Seinfeld, J. H., & Pandis, S. N. (1998). *Atmospheric chemistry and physics* (p. 809). New York: Wiley.

Tang, I. N., & Munkelwitz, H. R. (1994). Water activities, densities, and refractive indices of aqueous sulfates and sodium nitrate droplets of atmospheric importance. *Journal of Geophysical Research*, *99*, 18,801–18,808.

Wenny, B. N., Schafer, J. S., DeLuisi, J. J., Saxena, V. K., Barnard, W. F., Petropavlovskikh, I. V., & Vergamini, A. J. (1998). A study of regional aerosol radiative properties and effects on ultraviolet-B radiation. *Journal of Geophysical Research*, *103*, 17,083–17,097.

Wright, D.L. (2000). Retrieval of optical properties of atmospheric aerosols from moments of the particle size distribution. *Journal of Aerosol Science*, *31*, 1–18.

Wright, D. L., Kasibhatla, P. S., McGraw, R., & Schwartz, S. E. (2001). Description and evaluation of a six-moment aerosol microphysical module for use in atmospheric chemical transport models. *Journal of Geophysical Research*, in press.

Yu, S., Saxena, V. K., Wenny, B. N., DeLuisi, J. J., Yue, G. K., & Petropavlovskikh, I. V. (2000). A study of the aerosol radiative properties needed to compute direct forcing in the Southeastern US. *Journal of Geophysical Research*, *105*, 24,739–24,749.

Yue, G. K., Lu, J., Mohnen, V. A., Wang, P.-H., Saxena, V. K., & Anderson, J. (1997). Retrieving aerosol optical properties from moments of the particle size distribution. *Geophysical Research Letters*, *24*, 651–654.